ACS APPLIED NANO MATERIALS
Cite This: ACS Appl. Nano Mater. XXXX, XXX, XXX−XXX
Article
www.acsanm.org

3D Mapping of the Structural Transitions in Wrinkled 2D Membranes: Implications for Reconfigurable Electronics, Memristors, and Bioelectronic Interfaces

Kaustubh S. Panse, Shan Zhou, and Yingjie Zhang*

Department of Materials Science and Engineering and Frederick Seitz Materials Research Laboratory, University of Illinois, Urbana, Illinois 61801, United States

Supporting Information

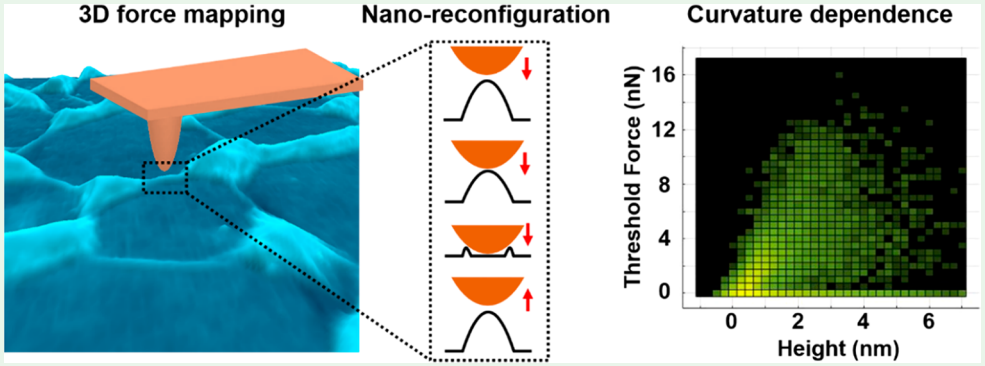

ABSTRACT: Bending and wrinkling occur widely in thin membrane materials, such as biomembranes, optical coatings, and two-dimensional materials. Such deformed structures can exhibit distinct mechanical responses compared to flat membranes. However, to date, mechanical characterization of membranes is mainly limited to the macroscopic level. The microscopic structure−mechanics relationship, key for rational materials design, remains elusive. Here we bridge this gap by mapping out the nanomechanical response of a model membrane system—wrinkled monolayer graphene. Using an atomic force microscope (AFM), we perform force−distance spectroscopy at each nanoscale spot to obtain a microscopic map. We observe a significant restoring force as the AFM tip pushes on graphene nanowrinkles. When the indenting force is higher than a threshold (a few nanonewtons), the wrinkles locally snap onto the SiO_2 substrate; after tip retraction, the wrinkles automatically restore their original shape. Through theoretical modeling and statistical analysis, we further find that nanoscale curvature enhances the effective stiffness and snapping threshold of atomically thin wrinkles. Our results can guide the rational design of mechanically reconfigurable materials and bioelectronic interfaces.

KEYWORDS: *nanowrinkle, mechanical reconfiguration, graphene, curvature, fast force mapping, atomic force microscopy*

INTRODUCTION

Because of the small or negligible bending stiffness, thin membrane materials tend to deform out of plane, forming various wrinkle structures.[1−26] Such structural curvature can strongly modulate the membrane's functionality. In biomembranes, for example, curvature is critical for controlling membrane phase ordering, regulating protein conformation, modulating intracellular traffic, and so on.[5−7] In engineered systems such as two-dimensional materials, wrinkles are ubiquitously formed during the standard materials processing and device fabrication processes.[8−13] On one hand, these wrinkles can induce electron scattering which is undesirable for nanoelectronics.[9−11] On the other hand, controlled wrinkle structures can be utilized for large area electronics and energy applications. It has been shown before that wrinkles and curvature effects in 2D materials can improve their flexibility and stretchability,[12−20] modulate the wettability,[21,22] enhance the photoresponsivity,[23] and facilitate electrochemical energy conversion and storage.[24−26] Recently, curved 2D materials have also been demonstrated to enable mechanically reconfigurable, multifunctional electronic and photonic devices.[27−29] Despite the wide interest in modulating the membrane mechanics via curvature engineering, to date the structure−mechanics relationship of thin membranes is still not well understood. So far, the mechanical response of these deformed structures has been measured mainly by stretching and/or compressing the membranes along the in-plane direction via macroscopic actuation.[12−20] It has been found that the membranes can adjust the in-plane pressure change by forming and releasing ripples/wrinkles. However, the local

Received: June 29, 2019
Accepted: September 6, 2019
Published: September 6, 2019

DOI: 10.1021/acsanm.9b01232
ACS Appl. Nano Mater. XXXX, XXX, XXX−XXX

mechanical properties of the buckled structures, such as strain and stiffness, have not been experimentally quantified.

While the bulk, flat membrane has high flexibility and low bending stiffness, continuum mechanics models predict that deformed structures with convex curvature have stronger effective stiffness.[30−34] According to these models, the membrane will be able to sustain a larger pressure as the radius of curvature decreases. At the scaling limit of a few nanometers, we expect a significant curvature-induced stiffness, if the system still obeys the laws of continuum mechanics. Such a strong curvature−mechanics correlation can facilitate the rational design of mechanically reconfigurable materials with 3D architecture[27,35−37] and bioelectronic interfaces with controlled interfacial mechanical coupling.[38−40]

To determine the nanoscale curvature−mechanics relationship, we use an AFM-based technique, fast force mapping (FFM), to simultaneously measure the membrane wrinkle structure and mechanical properties. FFM is performed by measuring a vertical force−distance curve at each nanoscale pixel and then scanning the surface to obtain a three-dimensional force map, which enables us to analyze both the topographic profile and mechanical response of the sample. In FFM, the vertical tip motion is sinusoidally modulated at a high rate of 300−1000 Hz, enabling the acquisition of 3D force maps in an experimentally feasible time scale. This is distinct from previous nanoindentation measurements that obtain single force curves at fixed spots on membranes.[41,42] In the past few years, FFM has been used to quantify the nanomechanical properties of biological cells[43−45] but has not been employed to measure thin membrane systems, to the best of our knowledge.

RESULTS AND DISCUSSION

We choose an atomically thin membrane, single-layer graphene, as a model system. Raman spectroscopy shows no observable defect-induced peak (Supporting Information, Figure S1), revealing a high structural quality of our graphene samples. To induce controlled curvature variation of the system, we adopt our previously used method and lay graphene on top of isolated SiO_2 nanospheres (20 nm diameter) on a flat SiO_2 substrate[46−48] (Figure 1a). As shown in the atomic force microscopy (AFM) image in Figure 1b, our sample consists of three main types of areas: (1) graphene wrinkles with a typical length in the scale of ∼100 nm and a height <10 nm, (2) flat graphene on planar SiO_2 substrate, and (3) protruded graphene wrapped on top of nanospheres. Such nanoscale variation of membrane curvature facilitates controlled nanomechanical studies.

We perform FFM on the wrinkled graphene by pushing down each spot to the lowest position and subsequently retracting the tip away (Figure 1c). During this process, we observe the cantilever deflection as a function of the scanner extension. From these signals, we extract the force (between the tip and the contacted area) as a function of the indentation. Here the force is obtained as the product of the cantilever deflection and the tip's spring constant, while the indentation is extracted as the difference between the scanner extension and the cantilever deflection, which represents the depth to which the tip pushes down on the local area of the sample (Figure S2).

Figure 2 shows the representative results of force−distance curves at different spots on the flat graphene and on wrinkles. The results on the flat area (Figure 2a−c) are typical for hard

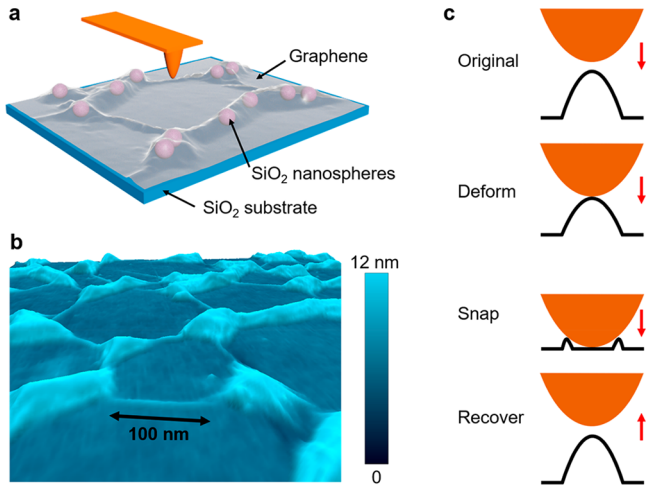

Figure 1. Sample structure and nanomechanical measurements. (a) Schematic of the sample structure and measurement setup. (b) A three-dimensional view of an experimental AFM height image of the wrinkled graphene on SiO_2/Si substrate. (c) Schematic of the FFM measurement. At each pixel, the tip approaches the sample, pushes on the local graphene area, and then lifts up. During this process, we find that the wrinkles deform, snap to the substrate, and eventually automatically recover their original shape.

surfaces, showing a sharp increase in force as soon as the tip hits the surface and an adhesion force in the range 1−3 nN as the tip retracts away. In contrast, the force curves on the wrinkle areas exhibit distinct behaviors, as shown in Figure 2d−f. As the tip pushes on the wrinkle, the force first increases sharply up to a threshold value (typically between 2 and 10 nN), and then the indentation jumps to the maximum value while the force slightly decreases, after which the force keeps increasing while the indentation remains unchanged. From the initial slope of force vs indentation (before the jump in indentation), we can extract an effective stiffness of 2−5 N/m. This is a large value considering the small tip−wrinkle contact area (estimated to be ∼10 nm^2, as discussed below) and the low bending rigidity of graphene (∼1.6 eV).[33,49,50] The sudden jump in indentation reveals that the local wrinkle area (underneath the tip) goes through a snapping transition and is abruptly pushed to the substrate by the tip when the force reaches a threshold. Because the stiffness of the SiO_2 substrate (a few kN/m)[51] is much higher than the spring constant of the AFM tip (1.5−5 N/m), the graphene cannot be pushed below the substrate surface. Through correlation analysis, we find that the total indentation depth of the wrinkles (obtained from FFM results) matches with the height of wrinkles obtained from AFM tapping mode image (Figure S3). This confirms that the wrinkles are indeed pushed onto the substrate when the force is above the snapping threshold. After indentation, the scanner is moved up to release the force. We find that the locally snapped wrinkle does not detach from the substrate before the force reaches zero (blue curves in Figure 2d−f), which is likely due to a finite adhesion force between the snapped graphene area and the SiO_2 substrate. Note that the areas of graphene wrapped on top of the nanospheres show no snapping behavior (Figure S4) because of two likely reasons: (1) the tip indentation is blocked by the underlying spheres; (2) there is a large tensile strain in graphene at these areas.[46]

Despite the presence of graphene−substrate adhesion, we find that most of the wrinkles recover to the original shape

DOI: 10.1021/acsanm.9b01232
ACS Appl. Nano Mater. XXXX, XXX, XXX−XXX

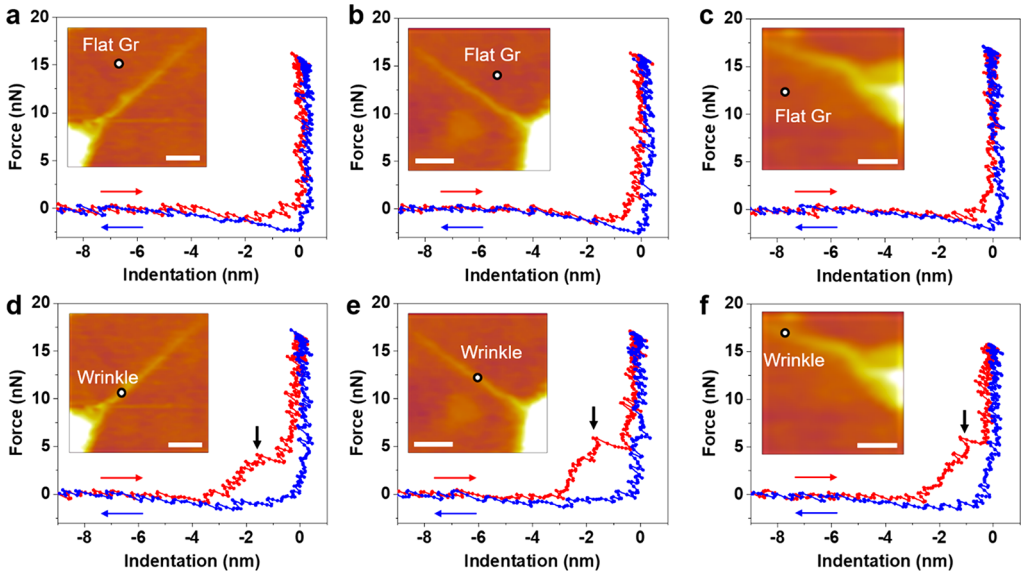

Figure 2. Representative force−indentation curves on flat graphene areas (a, b, c) and wrinkle spots (d, e, f). Black arrows in (d, e, f) mark the threshold snapping transition points. The insets in each panel show the AFM height images, where the circled spots mark the locations on which the force curves are obtained. Scale bars: 40 nm.

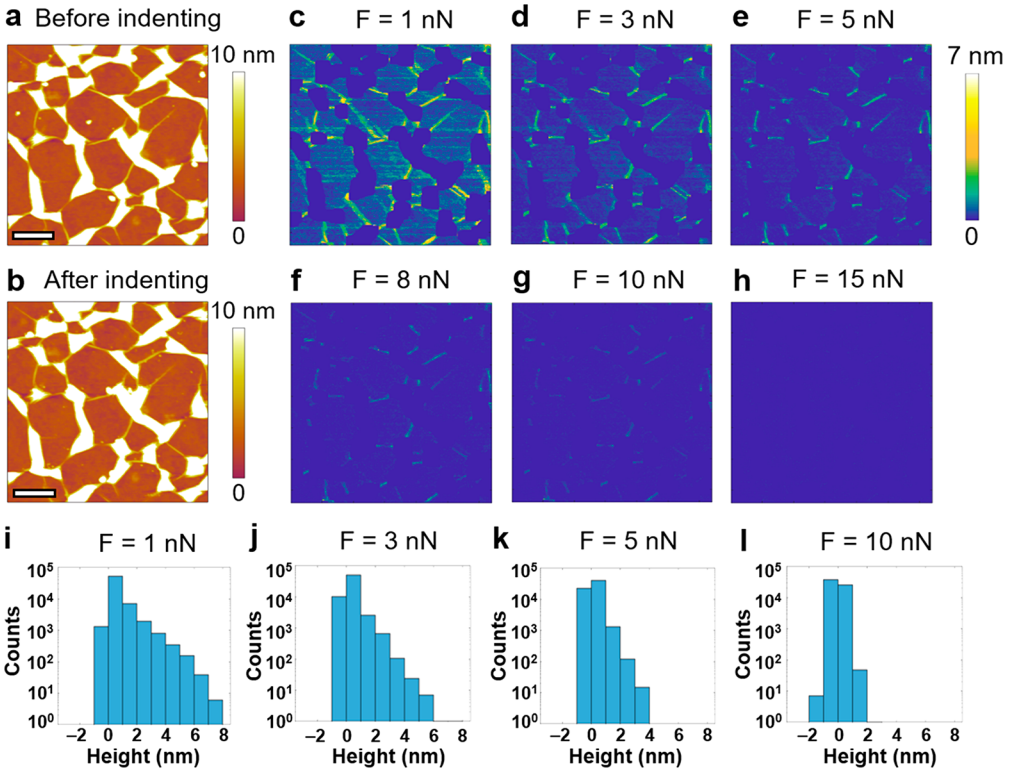

Figure 3. Height evolution of the wrinkles at different indentation forces. (a) and (b) are the tapping mode height images before and after the indentation. Scale bars: 200 nm. (c)−(h) show height images during the indentation at different force values (same area as (a) and (b)). Note that the areas at and near the nanospheres are masked and not analyzed, so that we can precisely and quantitatively analyze only the graphene nanowrinkles and flat graphene areas. (i)−(l) are the height histograms at different forces, corresponding to the height images in (c), (d), (e), and (g), respectively.

right after the tip retracts, as evident by comparing the tapping mode AFM height images before and after the FFM (Figure 3a,b). Although a "snapping transition" has been observed in graphene, previous studies have been focused on either the static structure of multilayer graphene on corrugated substrates[52] or the snapping of free-standing graphene induced by a uniform external force.[33,53,54] In these systems, with a size scale of a few micrometers, the snapped graphene either cannot restore the original shape or requires external energy to enable the recovery. In comparison, the automatic recovery capability of our graphene nanowrinkle structures is likely due to two factors: (1) larger stiffness induced by nanoscale curvature; (2)

DOI: 10.1021/acsanm.9b01232
ACS Appl. Nano Mater. XXXX, XXX, XXX−XXX

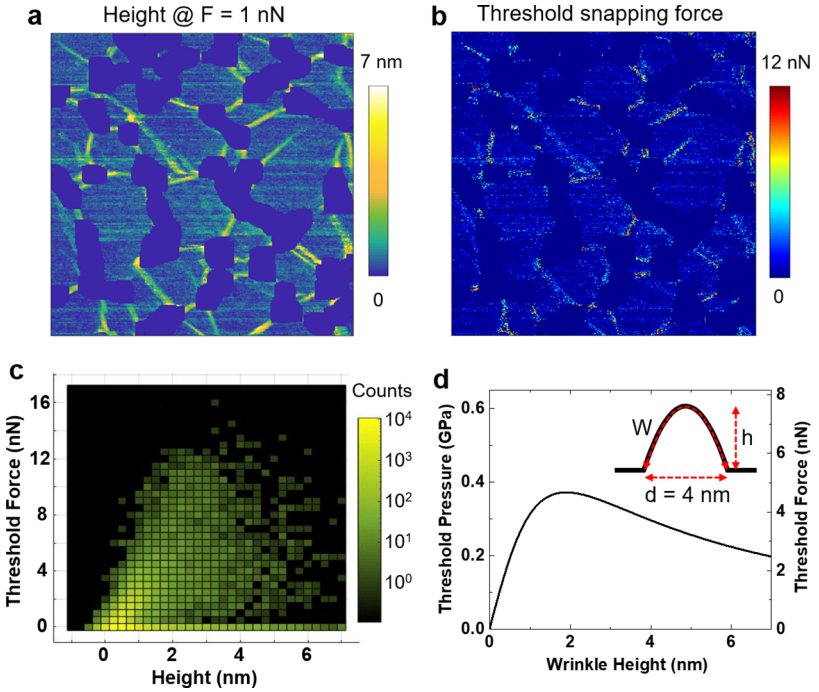

Figure 4. Threshold force analysis. (a) Height distribution at a force of 1 nN (same as Figure 3c, image size 1 μm × 1 μm). (b) Spatial distribution of the threshold snapping force, in the same area as (a). (c) Histogram of threshold force vs height, extracted from (a) and (b). (d) A continuum mechanics model predicting the dependence of threshold pressure/force on the wrinkle height. Inset is a schematic showing the key parameters used in the model.

the small snapping area (tip indents only on an ~10 nm^2 area of the wrinkle). Note that the thermal fluctuation of height in the nanowrinkles should be <0.1 Å at room temperature,[55] which is too small to induce snapping or recovery of the wrinkles.

To directly visualize the evolution of the wrinkle structure as a function of the tip indentation force, we extract the height maps of the sample at a series of different force set point values using the tip approaching part of the FFM curves. The results are shown in Figure 3c–h. Note that the areas on top of and near the SiO_2 nanospheres (~20 nm in diameter) are masked and not analyzed (see the Methods section for details), since in these areas the tip indentation is hindered by the nanospheres and the obtained force spectra do not represent the wrinkles' intrinsic mechanical property. As shown in Figure 3c, at a small force (1 nN), the wrinkles have nearly the same height as their original configuration (Figure 3a). As the force increases, the wrinkles gradually become lower in height (Figure 3d–h). At a force of 15 nN, the height image becomes flat (Figure 3h), revealing that the wrinkles are all pushed onto the substrate. Note that this series of height images is not obtained from contact mode AFM scanning (which can lead to lateral distortions due to friction), but rather extracted from the FFM results that more genuinely represent the mechanical response of the wrinkles as the tip vertically indents onto them.

The histogram of the height distribution at different forces, extracted from Figure 3c,d,e,g, is plotted in Figure 3i,j,k,l. As the force increases from 1 to 10 nN, the range of height distribution shrinks from ~0–7 to ~0–1 nm. These results further quantify the decreasing trend of the wrinkle height as the force increases and indicate that the snapping transition of the wrinkles has been mostly completed at a force of ~10 nN.

In addition to the height distribution at different force set points, we also analyze the characteristic force distribution. A key parameter of the force curves is the threshold force for the snapping transition. To quantify the threshold values, we take the derivative of the force vs indentation curve and extract the local minimum with the largest prominence as the snapping transition point (see the Methods section and Figure S5). The corresponding force at this transition point is obtained as the threshold force, which is mapped out in real space, as shown in Figure 4b. Comparing Figure 4a (height image at a small force set point of 1 nN) and Figure 4b, we can see that the graphene on all the flat SiO_2 substrate areas show nearly zero threshold force, i.e., no snapping transition. In most of the graphene wrinkle areas, we observe a finite threshold force (1–12 nN).

The simultaneously obtained height and threshold force maps enable a correlation analysis of these two parameters. We plot the correlation histogram in Figure 4c. We observe a large distribution of points at nearly zero height and zero threshold force corresponding to the flat graphene areas, a range of finite threshold force points with height between 0 and 7 nm corresponding to wrinkles, and a series of zero threshold force points with nonzero height corresponding to various features where snapping transition is not observed. It is worth mentioning that snapping behaviors are absent at the spots of poly(methyl methacrylate) (PMMA) which are residues from graphene transfer and cannot be clearly observed at some wrinkle spots due to the insufficient signal-to-noise ratio in the force curves. Given that the wrinkle width is nearly constant (~4 nm, Figure S6), an increase in height corresponds to an increase of curvature (decrease of the radius of curvature) of the wrinkles. In the height range of 0–2 nm, the threshold force is found to increase as the height increases, revealing that a finite curvature is required to induce the snapping transition. When the height is above 2 nm, the force distribution becomes very broad, preventing a quantitative analysis of the evolution trend of threshold force vs wrinkle height. Note that our

DOI: 10.1021/acsanm.9b01232
ACS Appl. Nano Mater. XXXX, XXX, XXX–XXX

experimentally measured narrow (a few nanometers wide) and long (>100 nm) wrinkle shape is consistent with previous simulations[56−58] and can be explained as a result of the balance of the internal strain of graphene, graphene−substrate adhesion, and graphene−substrate friction.

In macroscopic and micrometer-scale membrane systems, continuum mechanics models have been developed to explain the effect of convex curvature on the membranes' enhanced effective stiffness in response to external forces.[30−34] According to these models, the mechanical response of curved membranes depends on the convoluted effect of in-plane stress and out-of-plane bending; when the curvature is convex, the membrane will develop an in-plane compressive stress in response to out-of-plane compression, leading to an enhancement of the effective stiffness. A snapping transition occurs when the external force reaches the sum of the maximum compressive and bending force of the membrane. For the particular system of a curved membrane plate fixed at two sides, the threshold snapping pressure is found to be[34]

$$P_{th} = C_0 D \frac{1}{W^3}\left(\frac{W}{d}\right)^{11/8}\left(\frac{W}{d} - 1\right)^{1/2} \quad (1)$$

where C_0 = 253.4, D is the bending rigidity, W is the overall contour width of the curved membrane between the fixed sides, and d is the horizontal projection of W (horizontal distance between the two fixed sides). The inset in Figure 4d shows the schematic of a curved membrane where W, d, and h (wrinkle height) are labeled. The terms $1/W^3$ and W/d depend on the overall size and curvature of the deformed membrane, respectively. Smaller size and smaller radius of curvature lead to larger effective stiffness of the curved membrane and thus higher threshold pressure of the snapping transition.

For single-layer graphene, we have D = 1.6 eV.[34] In our graphene nanowrinkles, we assign d = 4 nm as estimated from scanning electron microscopy (SEM) images (Figure S6). To a first-order approximation, we assume the wrinkles have parabolic bending shape[34,48] and obtain the relation of W a function of d and h (see the Methods section). From eq 1 and the relationship between W and h, we obtain P_{th} as a function of h, as shown in Figure 4d. This continuum mechanics model predicts an increase in P_{th} as the wrinkle height increases from 0 to ∼2 nm due to the decrease of the radius of curvature (increase in W/d); as the height further increases, P_{th} starts to decrease, due to the increase in wrinkle size (decrease in $1/W^3$).

Comparing Figures 4c and 4d, we can see that our experimental results are roughly consistent with the continuum mechanics model. We observe a similar increase in threshold force/pressure as the wrinkle height increases from 0 to ∼2 nm, although it is hard to quantitatively compare the trend at higher height due to the large fluctuation in experimental results. Considering that the wrinkle's lateral width is ∼4 nm, we can estimate that the tip−wrinkle contact area is circular with a diameter of 4 nm. Using this area value, we convert the theoretical threshold pressure values to force, as shown in the right axis of Figure 4d. The magnitude of the force values agrees with the experimental results, revealing that the continuum mechanics model is sufficient to explain the high effective stiffness and large snapping transition pressure of nanoscale, atomically thin membrane wrinkles.

The size dependence of the curvature-induced stiffness can also be verified by comparing our work with previous studies of graphene microblisters. From the deflection vs pressure curves shown in refs 53 and 54, we can extract an effective stiffness per unit area in the scale of 10^{11}−10^{13} Pa/m. In comparison, our results show an effective stiffness of 2−5 N/m and a tip−wrinkle contact area of ∼10 nm^2, corresponding to an effective stiffness per unit area in the order of ∼10^{17} Pa/m. This higher effective stiffness (per unit area) is due to the smaller size of our nanowrinkles (a few nanometers wide) compared to the previously reported microblisters (∼3 μm), in agreement with our main conclusion that the effective stiffness scales up as the size goes down. The observed structure−mechanics relationship and the nanoscale enhancement of the effective stiffness in wrinkled 2D materials can greatly facilitate rational materials design for applications in robust, mechanically reconfigurable devices.

We expect the curvature-induced stiffness, snapping transition, and autorecovery effects to generally exist in other wrinkled 2D materials and other thin membrane materials, as predicted by the continuum mechanics model that contains no atomistic details (eq 1). For example, monolayer MoS_2 has a bending rigidity of ∼9.6 eV,[59,60] 6 times higher than that of graphene (1.6 eV). According to eq 1, we expect monolayer MoS_2 nanowrinkles to have a larger curvature-induced stiffness, and the snapping transition should occur at a threshold force that is ∼6 times higher than that of graphene, assuming the wrinkle size and curvature are the same.

CONCLUSIONS

In summary, through nanomechanical mapping, we observe high mechanical stiffness, snapping transitions, and automatic shape recovery effects in graphene nanowrinkles in response to local compressive force. We find that smaller wrinkle size and smaller radius of curvature both lead to larger effective stiffness and higher threshold snapping pressure. Given that nanoscale deformation and curvature widely exist in thin membranes, our results can serve as a general guidance to the understanding and design of membrane mechanics and pave the way for applications in reconfigurable mechanics, memristors, and bioelectronics.

METHODS

Sample Preparation. SiO_2 nanospheres with 20 nm diameter were purchased from nanoComposix.[46,47] The nanospheres are dispersed in water with a concentration of 5 mg/mL. We clean 300 nm SiO_2/Si by sonicating in acetone and isopropanol and then performing oxygen plasma. The nanospheres are drop-casted onto the SiO_2/Si substrate followed by blow-drying. Scanning electron microscopy images of the nanosphere coated substrates are shown in Figure S7, where we can see isolated single nanospheres or few-particle clusters. We purchase CVD graphene on Cu foil from ACS Material, LLC. Graphene is transferred onto the SiO_2 nanosphere/SiO_2/Si substrate by using a wet transfer technique described in our previous work.[46,47]

Atomic Force Microscopy (AFM). AFM measurements are performed using an Asylum Cypher ES AFM, where the sample is placed inside an environmental chamber purged with nitrogen gas. AFM tips were purchased from BudgetSensors, with model number Tap150Al-G. The spring constant (typically between 1.5 and 5 N/m) is measured via thermal tune of the AFM tips to ensure an accurate detection of the tip−sample interaction force. Fast force mapping (FFM) is performed with a Z rate (vertical force spectra) of 300−600 Hz and a horizontal pixel size of 2−4 nm. To verify that the magnitude of the Z rate does not affect the results, we measured individual force curves at a slower rate of 1 Hz. The results are shown in Figure S8, which we find to be similar to the FFM data.

DOI: 10.1021/acsanm.9b01232
ACS Appl. Nano Mater. XXXX, XXX, XXX−XXX

Scanning Electron Microscopy (SEM). SEM measurements are performed using a Hitachi S-4800 SEM, with an acceleration voltage of 5−10 kV and a working distance of ∼5 mm.

Calculation of the Wrinkle Contour Width. The contour width of the curved wrinkle W is obtained as a function of the lateral width d and the wrinkle height h by geometrical integration of the parabolic shape:

$$W = 2\left(\int_0^{d/2} \sqrt{1 + \left(\frac{dy}{dx}\right)^2}\, dx\right) = \frac{(4h/d\sqrt{16(h/d)^2 + 1}) + \ln(4h/d + \sqrt{16(h/d)^2 + 1})}{8(h/d)^2} h$$

where $y = ax^2$ is the equation of the parabola used to model the cross section of the wrinkle. Based on the above notation, $a = h/(d/2)^2$.

FFM Analysis. FFM data are analyzed by using MATLAB. We first extract the deflection vs scanner extension (*Ext*) curves for each pixel of the FFM result. For each curve, we sort the data in the ascending order of the *Ext* values and smooth the curve with 10 neighboring points. The force is obtained by multiplying the deflection and the measured spring constant of the cantilever (Figure S2). At a given force, the *Ext* value is extracted as the height and plotted in Figure 3c−h. To remove the tall regions near SiO_2 nanospheres, we use the height map at 1 nN (Figure 3c) to create a mask that covers all the features taller than 10 nm and their neighboring 13 × 13 points. The same mask is applied to the height images at other forces (Figure 3d−h).

To obtain the threshold snapping force, we first convert all the deflection vs *Ext* curves to force vs indentation curves (methods are shown in Figure S2). Then we take the first derivative of the force vs indentation curves and extract the local minimum with the largest prominence as the snapping transition point (Figure S5). The corresponding force at this transition point is extracted as the threshold force. The same mask to exclude the tall regions in the height map (Figure 3c−h) is used when plotting the threshold force map in Figure 4b.

■ ASSOCIATED CONTENT

Supporting Information

The Supporting Information is available free of charge on the ACS Publications website at DOI: 10.1021/acsanm.9b01232.

Figures S1−S8 (PDF)

■ AUTHOR INFORMATION

Corresponding Author

*E-mail yjz@illinois.edu.

ORCID

Shan Zhou: 0000-0002-6476-3280

Yingjie Zhang: 0000-0002-2704-8894

Author Contributions

K.S.P. and S.Z. contributed equally to this work.

Notes

The authors declare no competing financial interest.

■ ACKNOWLEDGMENTS

This work was supported by the University of Illinois at Urbana−Champaign. The experiments were performed in part in the Frederick Seitz Materials Research Laboratory Central Facilities and in the Carl R. Woese Institute for Genomic Biology at the University of Illinois. The authors acknowledge the use of facilities and instrumentation supported by NSF through the University of Illinois Materials Research Science and Engineering Center (DMR-1720633).

■ REFERENCES

(1) Lobkovsky, A.; Gentges, S.; Li, H.; Morse, D.; Witten, T. A. Scaling Properties of Stretching Ridges in a Crumpled Elastic Sheet. *Science* **1995**, *270*, 1482−1485.

(2) Cerda, E.; Mahadevan, L. Geometry and Physics of Wrinkling. *Phys. Rev. Lett.* **2003**, *90*, 074302.

(3) Choi, J. S.; Kim, J. S.; Byun, I. S.; Lee, D. H.; Lee, M. J.; Park, B. H.; Lee, C.; Yoon, D.; Cheong, H.; Lee, K. H.; Son, Y.-W.; Park, J. Y.; Salmeron, M. Friction Anisotropy-Driven Domain Imaging on Exfoliated Monolayer Graphene. *Science* **2011**, *333*, 607−610.

(4) Evensen, H. T.; Jiang, H.; Gotrik, K. W.; Denes, F.; Carpick, R. W. Transformations in Wrinkle Patterns: Cooperation Between Nanoscale Cross-Linked Surface Layers and the Submicrometer Bulk in Wafer-Spun, Plasma-Treated Polydimethylsiloxane. *Nano Lett.* **2009**, *9*, 2884−2890.

(5) Larsen, J. B.; Jensen, M. B.; Bhatia, V. K.; Pedersen, S. L.; Bjørnholm, T.; Iversen, L.; Uline, M.; Szleifer, I.; Jensen, K. J.; Hatzakis, N. S.; Stamou, D. Membrane Curvature Enables N-Ras Lipid Anchor Sorting to Liquid-Ordered Membrane Phases. *Nat. Chem. Biol.* **2015**, *11*, 192−194.

(6) Iversen, L.; Mathiasen, S.; Larsen, J. B.; Stamou, D. Membrane Curvature Bends the Laws of Physics and Chemistry. *Nat. Chem. Biol.* **2015**, *11*, 822−825.

(7) Roux, A.; Koster, G.; Lenz, M.; Sorre, B.; Manneville, J.-B.; Nassoy, P.; Bassereau, P. Membrane Curvature Controls Dynamin Polymerization. *Proc. Natl. Acad. Sci. U. S. A.* **2010**, *107*, 4141−4146.

(8) Chae, S. J.; Gunes, F.; Kim, K. K.; Kim, E. S.; Han, G. H.; Kim, S. M.; Shin, H.-J.; Yoon, S.-M.; Choi, J.-Y.; Park, M. H.; Yang, C. W.; Pribat, D.; Lee, Y. H. Synthesis of Large-Area Graphene Layers on Polynickel Substrate by Chemical Vapor Deposition: Wrinkle Formation. *Adv. Mater.* **2009**, *21*, 2328−2333.

(9) Katsnelson, M. I.; Geim, A. K. Electron Scattering on Microscopic Corrugations in Graphene. *Philos. Trans. R. Soc., A* **2008**, *366*, 195−204.

(10) Zhu, W.; Low, T.; Perebeinos, V.; Bol, A. A.; Zhu, Y.; Yan, H.; Tersoff, J.; Avouris, P. Structure and Electronic Transport in Graphene Wrinkles. *Nano Lett.* **2012**, *12*, 3431−3436.

(11) Ni, G. X.; Zheng, Y.; Bae, S.; Kim, H. R.; Pachoud, A.; Kim, Y. S.; Tan, C. L.; Im, D.; Ahn, J. H.; Hong, B. H.; Ozyilmaz, B. Quasi-Periodic Nanoripples in Graphene Grown by Chemical Vapor Deposition and its Impact on Charge Transport. *ACS Nano* **2012**, *6*, 1158−1164.

(12) Bao, W. Z.; Miao, F.; Chen, Z.; Zhang, H.; Jang, W. Y.; Dames, C.; Lau, C. N. Controlled Ripple Texturing of Suspended Grapheme and Ultrathin Graphite Membranes. *Nat. Nanotechnol.* **2009**, *4*, 562−566.

(13) Chen, Z.; Ren, W.; Gao, L.; Liu, B.; Pei, S.; Cheng, H. M. Three Dimensional Flexible and Conductive Interconnected Graphene Networks Grown by Chemical Vapor Deposition. *Nat. Mater.* **2011**, *10*, 424−428.

(14) Wang, Y.; Yang, R.; Shi, Z. W.; Zhang, L. C.; Shi, D. X.; Wang, E.; Zhang, G. Y. Super-Elastic Graphene Ripples for Flexible Strain Sensors. *ACS Nano* **2011**, *5*, 3645−3650.

(15) Nicholl, R. J.; Conley, H. J.; Lavrik, N. V.; Vlassiouk, I.; Puzyrev, Y. S.; Sreenivas, V. P.; Pantelides, S. T.; Bolotin, K. I. The Effect of Intrinsic Crumpling on the Mechanics of Free-Standing Graphene. *Nat. Commun.* **2015**, *6*, 8789.

(16) Wang, M. C.; Chun, S.; Han, R. S.; Ashraf, A.; Kang, P.; Nam, S. Heterogeneous, Three-Dimensional Texturing of Graphene. *Nano Lett.* **2015**, *15*, 1829−1835.

(17) Chen, P.-Y.; Sodhi, J.; Qiu, Y.; Valentin, T. M.; Steinberg, R. S.; Wang, Z.; Hurt, R. H.; Wong, I. Y. Multiscale Graphene Topographies Programmed by Sequential Mechanical Deformation. *Adv. Mater.* **2016**, *28*, 3564−3571.

(18) Lee, W. K.; Kang, J.; Chen, K. S.; Engel, C. J.; Jung, W. B.; Rhee, D.; Hersam, M. C.; Odom, T. W. Multiscale, Hierarchical Patterning of Graphene by Conformal Wrinkling. *Nano Lett.* **2016**, *16*, 7121−7127.

DOI: 10.1021/acsanm.9b01232
ACS Appl. Nano Mater. XXXX, XXX, XXX−XXX

(19) Xiao, Y.; Xu, Z.; Liu, Y.; Peng, L.; Xi, J.; Fang, B.; Guo, F.; Li, P.; Gao, C. Sheet Collapsing Approach for Rubber-like Graphene Papers. *ACS Nano* **2017**, *11*, 8092−8102.
(20) Carbone, M. G. P.; Manikas, A. C.; Souli, I.; Pavlou, C.; Galiotis, C. Mosaic Pattern Formation in Exfoliated Graphene by Mechanical Deformation. *Nat. Commun.* **2019**, *10*, 1572.
(21) Zang, J. F.; Ryu, S.; Pugno, N.; Wang, Q. M.; Tu, Q.; Buehler, M. J.; Zhao, X. H. Multifunctionality and Control of the Crumpling and Unfolding of Large-Area Graphene. *Nat. Mater.* **2013**, *12*, 321−325.
(22) Choi, J.; Mun, J.; Wang, M. C.; Ashraf, A.; Kang, S.; Nam, S. Hierarchical, Dual Scale Structures of Atomically-Thin MoS_2 for Tunable Wetting. *Nano Lett.* **2017**, *17*, 1756−1761.
(23) Kang, P.; Wang, M. C.; Knapp, P. M.; Nam, S. W. Crumpled Graphene Photodetector with Enhanced, Strain-Tunable, and Wavelength-Selective Photoresponsivity. *Adv. Mater.* **2016**, *28*, 4639−4645.
(24) Wen, Z.; Wang, X.; Mao, S.; Bo, Z.; Kim, H.; Cui, S.; Lu, G.; Feng, X.; Chen, J. Crumpled Nitrogen-Doped Graphene Nanosheets with Ultrahigh Pore Volume for High-Performance Supercapacitor. *Adv. Mater.* **2012**, *24*, 5610−5616.
(25) Wang, K.; Huang, B.; Lin, F.; Lv, F.; Luo, M.; Zhou, P.; Liu, Q.; Zhang, W.; Yang, C.; Tang, Y.; Yang, Y.; Wang, W.; Wang, H.; Guo, S. Wrinkled Rh_2P Nanosheets as Superior pH-Universal Electrocatalysts for Hydrogen Evolution Catalysis. *Adv. Energy Mater.* **2018**, *8*, 1801891.
(26) Wang, H.; Li, Y.; Li, Y.; Liu, Y.; Lin, D.; Zhu, C.; Chen, G.; Yang, A.; Yan, K.; Chen, H.; Zhu, Y.; Li, J.; Xie, J.; Xu, J.; Zhang, Z.; Vila, R.; Pei, A.; Wang, K.; Cui, Y. Wrinkled Graphene Cages as Hosts for High-Capacity Li Metal Anodes Shown by Cryogenic Electron Microscopy. *Nano Lett.* **2019**, *19*, 1326−1335.
(27) Kang, P.; Kim, K.-H.; Park, H.-G.; Nam, S. Mechanically Reconfigurable Architectured Graphene for Tunable Plasmonic Resonances. *Light: Sci. Appl.* **2018**, *7*, 17.
(28) Yang, C.; Huang, Y.; Cheng, H.; Jiang, L.; Qu, L. Rollable, Stretchable, and Reconfigurable Graphene Hygroelectric Generators. *Adv. Mater.* **2019**, *31*, 1805705.
(29) Lee, S.; Kim, J. T.; Song, Y.-W. Graphene-Incorporated Soft Capacitors for Mechanically Adjustable Electro-Optic Modulators. *ACS Appl. Mater. Interfaces* **2018**, *10*, 40781−40788.
(30) Pogorelov, A. V. *Bending of Surfaces and Stability of Shells*, 1st ed.; American Mathematical Society: Providence, RI, 1988; Vol. 72.
(31) Paulsen, J. D.; Hohlfeld, E.; King, H.; Huang, J.; Qiu, Z.; Russell, T. P.; Menon, N.; Vella, D.; Davidovitch, B. Curvature-Induced Stiffness and the Spatial Variation of Wavelength in Wrinkled Sheets. *Proc. Natl. Acad. Sci. U. S. A.* **2016**, *113*, 1144−1149.
(32) Bende, N. P.; Evans, A. A.; Innes-Gold, S.; Marin, L. A.; Cohen, I.; Hayward, R. C.; Santangelo, C. D. Geometrically Controlled Snapping Transitions in Shells with Curved Creases. *Proc. Natl. Acad. Sci. U. S. A.* **2015**, *112*, 11175−11180.
(33) Lindahl, N.; Midtvedt, D.; Svensson, J.; Nerushev, O. A.; Lindvall, N.; Isacsson, A.; Campbell, E. E. B. Determination of the Bending Rigidity of Graphene via Electrostatic Actuation of Buckled Membranes. *Nano Lett.* **2012**, *12*, 3526−3531.
(34) Yamaletdinov, R. D.; Ivakhnenko, O. V.; Sedelnikova, O. V.; Shevchenko, S. N.; Pershin, Y. V. Snap-Through Transition of Buckled Graphene Membranes for Memcapacitor Applications. *Sci. Rep.* **2018**, *8*, 3566.
(35) Zheng, X.; Lee, H.; Weisgraber, T. H.; Shusteff, M.; DeOtte, J.; Duoss, E. B.; Kuntz, J. D.; Biener, M. M.; Ge, Q.; Jackson, J. A.; Kucheyev, S. O.; Fang, N. X.; Spadaccini, C. M. Ultralight, Ultrastiff Mechanical Metamaterials. *Science* **2014**, *344*, 1373−1377.
(36) Blees, M. K.; Barnard, A. W.; Rose, P. A.; Roberts, S. P.; McGill, K. L.; Huang, P. Y.; Ruyack, A. R.; Kevek, J. W.; Kobrin, B.; Muller, D. A.; McEuen, P. L. Graphene Kirigami. *Nature* **2015**, *524*, 204−207.
(37) Cui, H.; Hensleigh, R.; Yao, D.; Maurya, D.; Kumar, P.; Kang, M. G.; Priya, S.; Zheng, X. Three-Dimensional Printing of Piezoelectric Materials with Designed Anisotropy and Directional Response. *Nat. Mater.* **2019**, *18*, 234−241.
(38) Dagdeviren, C.; Javid, F.; Joe, P.; von Erlach, T.; Bensel, T.; Wei, Z.; Saxton, S.; Cleveland, C.; Booth, L.; McDonnell, S.; Collins, J.; Hayward, A.; Langer, R.; Traverso, G. Flexible Piezoelectric Devices for Gastrointestinal Motility Sensing. *Nat. Biomed. Eng.* **2017**, *1*, 807−817.
(39) Chortos, A.; Liu, J.; Bao, Z. Pursuing Prosthetic Electronic Skin. *Nat. Mater.* **2016**, *15*, 937−950.
(40) Cheng, C.; Zhang, J.; Li, S.; Xia, Y.; Nie, C.; Shi, Z.; CuellarCamacho, J. L.; Ma, N.; Haag, R. A Water-Processable and Bioactive Multivalent Graphene Nanoink for Highly Flexible Bioelectronic Films and Nanofibers. *Adv. Mater.* **2018**, *30*, 1705452.
(41) Lee, C.; Wei, X.; Kysar, J. W.; Hone, J. Measurement of the Elastic Properties and Intrinsic Strength of Monolayer Graphene. *Science* **2008**, *321*, 385−388.
(42) Lee, G.-H.; Cooper, R. C.; An, S. J.; Lee, S.; van der Zande, A.; Petrone, N.; Hammerberg, A. G.; Lee, C.; Crawford, B.; Oliver, W.; Kysar, J. W.; Hone, J. High-Strength Chemical-Vapor-Deposited Graphene and Grain Boundaries. *Science* **2013**, *340*, 1073−1076.
(43) Alsteens, D.; Newton, R.; Schubert, R.; Martinez-Martin, D.; Delguste, M.; Roska, B.; Müller, D. J. Nanomechanical Mapping of First Binding Steps of a Virus to Animal Cells. *Nat. Nanotechnol.* **2017**, *12*, 177−183.
(44) Dufrenê, Y. F. Microbial Nanoscopy: Breakthroughs, Challenges, and Opportunities. *ACS Nano* **2017**, *11*, 19−22.
(45) Krieg, M.; Flaschner, G.; Alsteens, D.; Gaub, B. M.; Roos, W. H.; Wuite, G. J. L.; Gaub, H. E.; Gerber, C.; Dufrene, Y. F.; Müller, D. J. Atomic Force Microscopy-Based Mechanobiology. *Nat. Rev. Phys.* **2019**, *1*, 41−57.
(46) Zhang, Y.; Heiranian, M.; Janicek, B.; Budrikis, Z.; Zapperi, S.; Huang, P. Y.; Johnson, H. T.; Aluru, N. R.; Lyding, J. W.; Mason, N. Strain Modulation of Graphene by Nanoscale Substrate Curvatures: A Molecular View. *Nano Lett.* **2018**, *18*, 2098−2104.
(47) Zhang, Y.; Kim, Y.; Gilbert, M. J.; Mason, N. Electronic Transport in a Two-Dimensional Superlattice Engineered via Self-Assembled Nanostructures. *npj 2D Mater. Appl.* **2018**, *2*, 31.
(48) Yamamoto, M.; Pierre-Louis, O.; Huang, J.; Fuhrer, M.; Einstein, T.; Cullen, W. The Princess and the Pea" at the Nanoscale: Wrinkling and Delamination of Graphene on Nanoparticles. *Phys. Rev. X* **2012**, *2*, 041018.
(49) Zhang, D. B.; Akatyeva, E.; Dumitrică, T. Bending Ultrathin Graphene at the Margins of Continuum Mechanics. *Phys. Rev. Lett.* **2011**, *106*, 255503.
(50) Wei, Y.; Wang, B.; Wu, J.; Yang, R.; Dunn, M. L. Bending Rigidity and Gaussian Bending Stiffness of Single-Layered Graphene. *Nano Lett.* **2013**, *13*, 26−30.
(51) Li, H.; Vlassak, J. J. Determining the Elastic Modulus and Hardness of an Ultra-thin Film on a Substrate using Nanoindentation. *J. Mater. Res.* **2009**, *24*, 1114−1126.
(52) Scharfenberg, S.; Mansukhani, N.; Chialvo, C.; Weaver, R. L.; Mason, N. Observation of a Snap-Through Instability in Graphene. *Appl. Phys. Lett.* **2012**, *100*, 021910.
(53) Boddeti, N. G.; Liu, X.; Long, R.; Xiao, J.; Bunch, J. S.; Dunn, M. L. Graphene Blisters with Switchable Shapes Controlled by Pressure and Adhesion. *Nano Lett.* **2013**, *13*, 6216−6221.
(54) Liu, X.; Boddeti, N. G.; Szpunar, M. R.; Wang, L.; Rodriguez, M. A.; Long, R.; Xiao, J.; Dunn, M. L.; Bunch, J. S. Observation of Pull-In Instability in Graphene Membranes under Interfacial Forces. *Nano Lett.* **2013**, *13*, 2309−2313.
(55) Ahmadpoor, F.; Wang, P.; Huang, R.; Sharma, P. Thermal Fluctuations and Effective Bending Stiffness of Elastic Thin Sheets and Graphene: A Nonlinear Analysis. *J. Mech. Phys. Solids* **2017**, *107*, 294−319.
(56) Zhang, K.; Arroyo, M. Understanding and Strain-Engineering Wrinkle Networks in Supported Graphene through Simulations. *J. Mech. Phys. Solids* **2014**, *72*, 61−74.
(57) Zhang, K.; Arroyo, M. Coexistence of Wrinkles and Blisters in Supported Graphene. *Extreme Mech. Lett.* **2017**, *14*, 23−30.
(58) Zhang, K.; Arroyo, M. Adhesion and Friction Control Localized Folding in Supported Graphene. *J. Appl. Phys.* **2013**, *113*, 193501.

DOI: 10.1021/acsanm.9b01232
ACS Appl. Nano Mater. XXXX, XXX, XXX−XXX

(59) Jiang, J.-W.; Qi, Z.; Park, H. S.; Rabczuk, T. Elastic Bending Modulus of Single-Layer Molybdenum Disulfide (MoS_2): Finite Thickness Effect. *Nanotechnology* **2013**, *24*, 435705.
(60) Lai, K.; Zhang, W.-B.; Zhou, F.; Zeng, F.; Tang, B.-Y. Bending Rigidity of Transition Metal Dichalcogenide Monolayers from First-Principles. *J. Phys. D: Appl. Phys.* **2016**, *49*, 185301.

DOI: 10.1021/acsanm.9b01232
ACS Appl. Nano Mater. XXXX, XXX, XXX−XXX